

Article

Real Space and Time Imaging of Collective Headgroup Dipole Motions in Zwitterionic Lipid Bilayers

Dima Bolmatov ^{1,2,*} , C. Patrick Collier ³, Dmitry Zav'yalov ⁴, Takeshi Egami ^{1,2,5,6}  and John Katsaras ^{1,2,7}¹ Department of Physics and Astronomy, University of Tennessee, Knoxville, TN 37996, USA² Shull-Wollan Center, Oak Ridge National Laboratory, Oak Ridge, TN 37831, USA³ Center for Nanophase Materials Sciences, Oak Ridge National Laboratory, Oak Ridge, TN 37831, USA⁴ Department of Physics, Volgograd State Technical University, Volgograd 400005, Russia⁵ Department of Materials Science and Engineering, The University of Tennessee, Knoxville, TN 37916, USA⁶ Materials Science and Technology Division, Oak Ridge National Laboratory, Oak Ridge, TN 37831, USA⁷ Sample Environment Group, Neutron Scattering Division, Oak Ridge National Laboratory, Oak Ridge, TN 37831, USA

* Correspondence: dbolmato@utk.edu or bolmatovd@ornl.gov

Abstract: Lipid bilayers are supramolecular structures responsible for a range of processes, such as transmembrane transport of ions and solutes, and sorting and replication of genetic materials, to name just a few. Some of these processes are transient and currently, cannot be visualized in real space and time. Here, we developed an approach using 1D, 2D, and 3D Van Hove correlation functions to image collective headgroup dipole motions in zwitterionic phospholipid bilayers. We show that both 2D and 3D spatiotemporal images of headgroup dipoles are consistent with commonly understood dynamic features of fluids. However, analysis of the 1D Van Hove function reveals lateral transient and re-emergent collective dynamics of the headgroup dipoles—occurring at picosecond time scales—that transmit and dissipate heat at longer times, due to relaxation processes. At the same time, the headgroup dipoles also generate membrane surface undulations due a collective tilting of the headgroup dipoles. A continuous intensity band of headgroup dipole spatiotemporal correlations—at nanometer length and nanosecond time scales—indicates that dipoles undergo stretching and squeezing elastic deformations. Importantly, the above mentioned intrinsic headgroup dipole motions can be externally stimulated at GHz-frequency scale, enhancing their flexoelectric and piezoelectric capabilities (i.e., increased conversion efficiency of mechanical energy into electric energy). In conclusion, we discuss how lipid membranes can provide molecular-level insights about biological learning and memory, and as platforms for the development of the next generation of neuromorphic computers.

Keywords: zwitterionic lipid bilayers; POPC; DPPC; headgroup dipoles; collective dipole motions; Van Hove correlation functions; heat transfer; surface undulations; piezoelectricity; flexoelectricity



check for updates

Citation: Bolmatov, D.; Collier, C.P.; Zav'yalov, D.; Egami, T.; Katsaras, J. Real Space and Time Imaging of Collective Headgroup Dipole Motions in Zwitterionic Lipid Bilayers. *Membranes* **2023**, *13*, 442. <https://doi.org/10.3390/membranes13040442>

Academic Editor: Francisco Monroy

Received: 28 February 2023

Revised: 5 April 2023

Accepted: 14 April 2023

Published: 18 April 2023



Copyright: © 2023 by the authors. Licensee MDPI, Basel, Switzerland. This article is an open access article distributed under the terms and conditions of the Creative Commons Attribution (CC BY) license (<https://creativecommons.org/licenses/by/4.0/>).

1. Introduction

The study of collective molecular motions in hydrated phospholipid bilayers is a challenging area of science [1–3]. Although almost all liquid crystalline lipid bilayers undergo large molecular displacements, their intermolecular interactions are lipid specific [4–7]. In biological membranes, lipids are in constant motion—due to thermal energy—and their movements impact their physical properties, such as bilayer viscosity, energy and heat transfer, lipid diffusion, and overall morphology [8–12]. Importantly, lipid bilayers are the underlying structures of biological membranes and define the cell's extracellular and intracellular environments [13,14], and enable a range of biological processes [15].

Compared to other lipid bilayer dynamics, collective molecular motions, at their fundamental time and length scales, have been less studied experimentally [16–20]. In contrast, there have been considerable theoretical developments and analytical models that have

focused on understanding membrane collective motions [21–24]. However, almost without exception, these developments have been implemented in reciprocal space, making them somewhat cumbersome. On the other hand, demand for the development of theoretical and analytical frameworks using real spatial and temporal analyses at fundamental length and time scales, has been growing.

Zwitterionic lipid bilayers (see Figure 1) contain both positive (choline, blue) and negative (phosphate, orange) functional groups, resulting in a relatively high dipole moment at physiological pH [25–28]. Phospholipids such as 1-palmitoyl-2-oleoyl-*sn*-glycero-3-phosphocholine (POPC, 16:0/18:1 PC) and 1,2-dipalmitoyl-*sn*-glycero-3-phosphocholine (DPPC, 16:0/16:0 PC) spontaneously self assemble into bilayers in the presence of water (Figure 1), with their hydrophobic acyl tails forming the bilayer’s hydrophobic core, while their headgroups interact with the aqueous phase [29]. Both lipids occur naturally, and are involved in different cellular processes on length scales ranging from the nanometer to the micrometer [30–34].

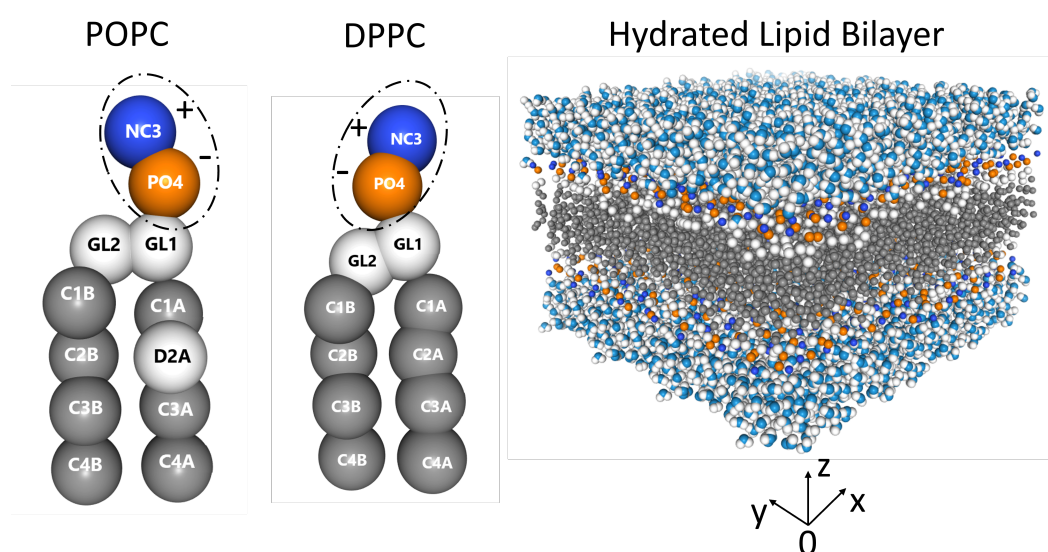


Figure 1. From left to right: POPC (16:0/18:1 PC), DPPC (16:0/16:0 PC), and a hydrated PC bilayer. Dashed ellipses around the POPC and DPPC phospholipid headgroups highlighting their positive charged choline (blue) and negative charged phosphate (orange) groups. The lipid bilayer is fully hydrated with the hydrophilic PC headgroups interacting with polar water molecules, which continuously experience the formation and breakup of hydrogen bonds at picosecond time scales [35–37].

Here, we developed an approach using the Van Hove correlation function in one, two, and three dimensions (1D, 2D, and 3D, respectively) to study the spatial and temporal correlations of zwitterionic PC headgroup dipoles. X-ray and neutron scattering techniques such as, diffraction have extensively been used to study the structural organization of lipids in biomembranes [38–40], including spatial lipid-lipid pair distribution functions and snapshot-like time evolution of their spatial correlations. Although useful, such information alone is insufficient for the understanding of collective dynamics and relaxation processes, which contain both spatial and temporal correlations.

We show that in 2D and 3D, the spatiotemporal images of collective motions are consistent with experimentally observed, common dynamic features associated with fluids. However, in 1D, analysis of the Van Hove function revealed lateral transient and re-emergent picosecond dynamics of the headgroup dipoles that transmit and subsequently dissipate heat. Importantly, the PC headgroup dipoles also generate slower membrane surface undulations—due to collective dipole tilting—and can undergo both stretching and squeezing elastic deformations. In theory, the headgroup dipole motions can also be externally stimulated at GHz-frequency scale, enhancing their piezoelectric capabilities (i.e., increased conversion efficiency of mechanical energy into electric energy).

2. Materials and Methods

2.1. Coarse-Grained Molecular Dynamics (MD) Simulations

We performed MD simulations using GROMACS (<http://www.gromacs.org>, accessed on 4 July 2022) and the MARTINI 2.2p force field [41]. A square model membrane with periodic boundary conditions was built using the CHARMM-GUI [42,43]. The number of lipids in each bilayer leaflet was 512, with a 22 Å water layer thickness on either side of the bilayer membrane. Pressure was set to 1 bar at 37 °C. The MD procedure was performed using the following three steps: (1) During the first simulation stage, the system energy was minimized by minimizing the intermolecular forces; (2) The system was brought into thermodynamic equilibrium using the NVT canonical ensemble, where T is the absolute temperature, N is the number of atoms, and V is the volume. The Thermostat V-Rescale with a time-constant of 1 ps was used for all the simulations, and the groups of atoms belonging to water and lipids were thermalized separately. Thermalization took place over 30 ns in steps of 20 fs; and (3) During the production stage, the system was in the NPT ensemble using the V-Rescale thermostat with a coupling time constant of 12 ps for the barostat. The simulation was carried out for 6 ns, in 20 fs increments. For the second and third simulation steps, van der Waals interactions were cut off at 1.1 nm and the electrostatic interactions, using the PME algorithm, were cut off at 1.2 nm.

2.2. 3D, 2D, 1D Van Hove Correlation Functions

The Van Hove correlation function describes the probability density of finding a particle A at a distance r and time t , when a particle B is at time $t = 0$ [44,45]. Previously, Van Hove function analysis has been used to analyze ultrafast real space dynamics of liquids using inelastic X-ray scattering [46–49]. Below, we define the Van Hove correlation function in 1D, 2D, and 3D to study the spatiotemporal collective motions of PC headgroup dipoles associated with POPC and DPPC lipid bilayers.

The Van Hove correlation function has two independent terms, i.e., a self part that describes diffusion properties of a particle in a local neighborhood, and a distinct part that describes collective properties of a particle correlated with neighboring particles [45]. Below, we define Van Hove correlation functions which contain both self and distinct parts.

The 3D Van Hove correlation function, $G^{3D}(r, t)$, which describes the distribution of A particles relative to B particles in a given volume, can be written as follows:

$$G_{AB}^{3D}(r, t) = \frac{V}{4\pi r^2 N_A N_B} \sum_{i,j} \delta(r - |\mathbf{r}_i^A(t) - \mathbf{r}_j^B(0)|_{3D}), \quad (1)$$

where $|\mathbf{r}_i^A(t) - \mathbf{r}_j^B(0)|_{3D}$ is the distance between particles i and j , with types A and B, respectively. $N_A(N_B)$ is the number of A(B) particles, t is the time, and V is the volume. Analogously, the 2D Van Hove correlation function $G^{2D}(r, t)$ can be written as:

$$G_{AB}^{2D}(r, t) = \frac{S}{2\pi r N_A N_B} \sum_{i,j} \delta(r - |\mathbf{r}_i^A(t) - \mathbf{r}_j^B(0)|_{2D}), \quad (2)$$

$|\mathbf{r}_i^A(t) - \mathbf{r}_j^B(0)|_{2D}$ is the distance between particles i and j with particle types A and B, respectively, in a given plane where S is the area of the system.

Finally, we define the 1D Van Hove correlation function $G^{1D}(r, t)$ as:

$$G_{AB}^{1D}(r, t) = \frac{L}{N_A N_B} \sum_{i,j} \delta(r - |\mathbf{r}_i^A(t) - \mathbf{r}_j^B(0)|_{1D}), \quad (3)$$

where $|\mathbf{r}_i^A(t) - \mathbf{r}_j^B(0)|_{1D}$ is the distance between the i and j particles with particle types A and B, respectively, along a given axis, where L is the length of the system along the axis.

For all Van Hove correlation functions, the headgroup bilayer (Figure 1) position, \mathbf{r}_i^A , is the center of mass of the i th choline (NC3-bead), and position \mathbf{r}_j^B is the center of mass of

the phosphate (PO_4 -bead) group. Thereafter, we will use the following notations: $G_{NP}^{1D}(r, t)$, $G_{NP}^{2D}(r, t)$, and $G_{NP}^{3D}(r, t)$. We would like to clarify that we used the phosphate bead as the $\mathbf{r}(0)$ of the Van Hove function and not the choline bead. We should also point out, that the difference between the choline and the phosphate bead $\mathbf{r}(0)$ is minimal, as such, we did not elaborate further on this point in the manuscript.

3. Results

3.1. Spatiotemporal Imaging of Collective Headgroup Dipole Motions and Relaxation Processes in Hydrated Phospholipid Bilayers

POPC and DPPC bilayers differ only in the chemistry of their acyl chains namely, DPPC has two 16:0 chains, while POPC has a 16:0 chain at its sn-1 position and an 18:1 at its sn-2 position. However, the presence of a double bond in the case of POPC (Figure 1), causes its physicochemical properties to be different from those of DPPC. As a result, compared to DPPC, POPC bilayers are more disordered and have a much lower gel-to-liquid-crystalline phase transition temperature (41 °C for DPPC vs. −2 °C for POPC)—at approximately 37 °C, DPPC bilayers undergo a so-called gel to ripple phase transition [50].

The Van Hove function captures spatiotemporal correlations in the form of particle density fluctuations and as such, can be used to directly access density fluctuations measured via inelastic neutron scattering (INS) [51]. Figure 2 displays 2D and 3D Van Hove correlation functions (see Equations (1) and (2)) of POPC (a,b), and DPPC (c,d) headgroup dipoles, whose ultrafast dynamic behavior is consistent with what has been previously observed in fluids by IXS [46–49] and INS [51]. For both POPC and DPPC bilayers, headgroup dipoles have sharp intensity peaks located at ~0.45 nm, consistent with nearest neighbor chain-chain distances observed in PC bilayers (~0.4 nm). The red sharp peaks (in the normalized intensity scale bars located to the right of Figure 2) indicate that the PC headgroups experience rattling or “cage-like” dynamics in the first 2–4 ps, followed by a long lasting relaxation process, i.e., the intensity drops down from “red” to “white”. Interestingly, $G_{NP}^{2D}(r, t)$ correlation functions are more informative than $G_{NP}^{3D}(r, t)$ (see Figure 2), i.e., Figure a,c vs. Figure b,d. Specifically, the “caging phase” of the collective dynamics associated with the headgroup dipoles undergoes a clear transition (white arcs around the red peaks), and the traces of the relaxation phase are more detailed and last significantly longer. As such, it is physically justified to independently analyze the behavior of the $G_{NP}^{1D}(r, t)$ correlation function of the POPC and DPPC headgroup dipoles, both laterally and along the z-axis.

Figure 3 shows 1D Van Hove correlation functions (see Equation (3)) of POPC (a,b) and DPPC (c,d) headgroup dipoles undergoing lateral motion. Interestingly, analysis of the Van Hove correlation function in reduced dimensions provides additional insights, which are consistent with previous IXS results from oriented lipid bilayers [52]. Specifically, 1D analysis of lateral headgroup dipole motions reveals spatiotemporal correlations that are buried in higher dimensions. It is worth noting that $G_{NP}^{1D}(r, t)$ correlation functions are identical along any direction within the bilayer plane (Figure 1), since both POPC and DPPC membranes are isotropically disordered in the lateral direction, as well as along the “x” and “y” axes. Furthermore, over short times (0–25 ps), dipoles in the first coordination shell experience the strongest caging events (Figure 3a,c), slowly relaxing at longer times with well-defined attenuating traces. During the caging phase, lipids are capable of supporting both longitudinal collective motions, in the form of compression waves, and transverse collective displacements, in the form of shear waves. This means that mechanical stress is localized, dynamically squeezing both the lipids and the bound interfacial water molecules, thereby making the bilayer elastic [53,54]. At longer times, transverse restoring forces become negligible, i.e., undergoing the elastic-to-viscous crossover [53], and lipid molecules are no longer responsive to shear waves, resulting in a viscous local lipid environment. Therefore, the localized mechanical stress is forced to propagate forward due to continuous impact from compression waves. Of note, these observations are consistent with previously reported reciprocal space data from IXS [54].

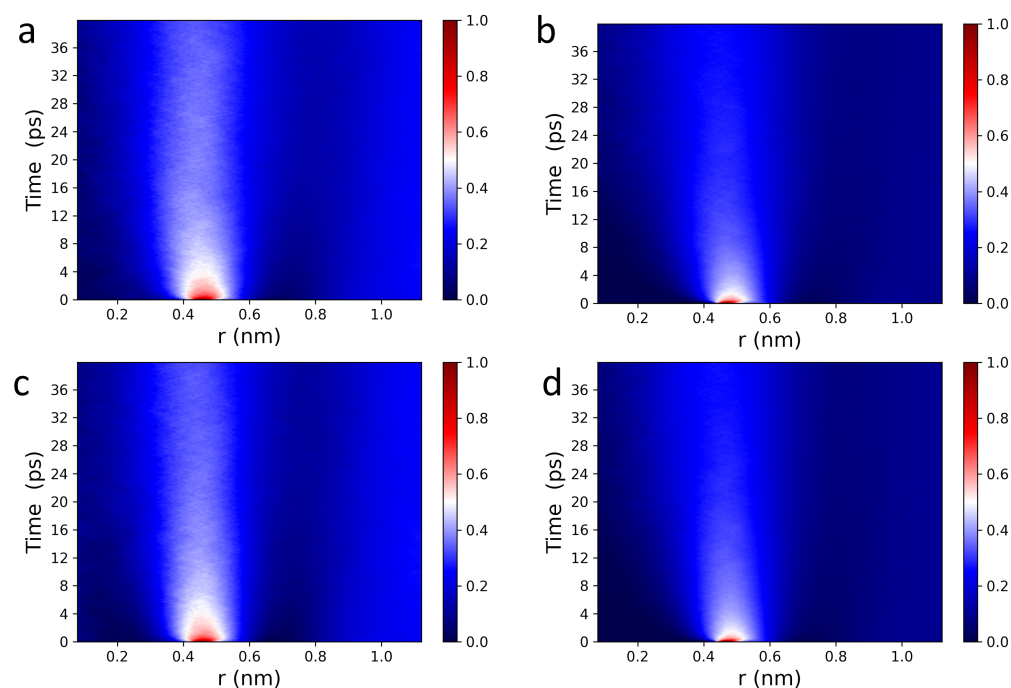


Figure 2. 2D and 3D Van Hove correlation functions (see Equations (2) and (3)) of POPC (a,b) and DPPC (c,d) PC headgroup dipoles consist of choline-phosphate functional groups (see Figure 1). (a,c) $G_{NP}^{2D}(r, t)$ and (b,d) $G_{NP}^{3D}(r, t)$ correlation functions of PC headgroups at 37 °C contain all of the major spectral features of liquid systems measured using IXS [46–49] and INS [51].

Of note, unlike in simple liquids [55,56], the mechanical stress in phospholipid membranes propagates laterally, bouncing back and forth between neighboring local lipid environments (Figure 3a,c). Extending this in space and time (Figure 3b,d) reveals a mesh-like vibrational pattern, reminiscent of the surface of a “boiling” viscous liquid [54]. This spatiotemporal image—coexistence of high intensity (compressed) and low intensity (diffused) regions—also lends further evidence supporting the mechanism for passive transmembrane transport of small molecules and solutes revealed by IXS experiments [52]. Due to increased disorder, POPC lateral correlations are also less intense than those of DPPC bilayers, as highlighted by the randomly-circled red intensity peaks in Figure 3 [(b) vs. (d)] and Figure 4 [(a) vs. (b)]. Furthermore, Figure 4 shows a periodic time evolution of the spatiotemporal correlation intensity peak within the first coordination shell generated by POPC (a) and DPPC (b) lipid headgroups, respectively. The insets to the figure, generated using Fourier transforms, show power spectra of POPC and DPPC headgroup dipoles ranging between ~ 1 GHz and ~ 30 GHz. Importantly, the wiggling patterns of the collective lateral headgroup dipole motions—represented in the dark blue low intensity areas—are clearly featured. For instance, arising at ~ 400 ps along $r = 0.8$ nm, potentially coupling to bilayer surface undulations existing at slower times and frequencies.

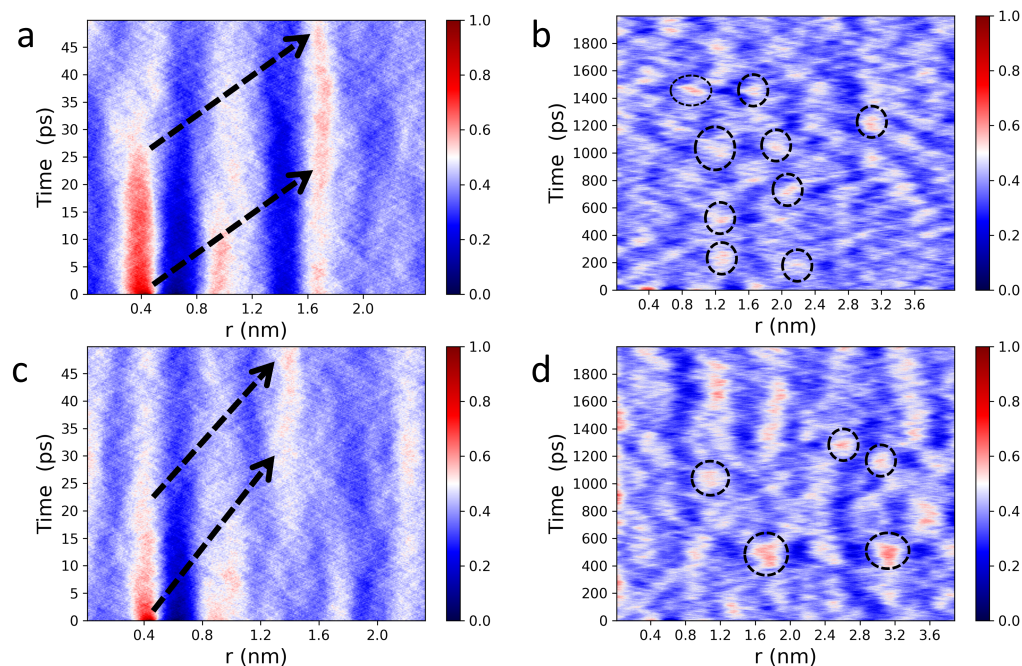


Figure 3. Lateral, spatiotemporal pair correlations for POPC (a,b) and DPPC (c,d) headgroup dipoles calculated from Equation (1). Wide, red line intensity peaks (a,c) indicate strongly correlated “cage-like” dynamics, followed by smooth relaxation processes (nearly straight white traces) along the first, second, and third coordination shells. Black arrows indicate the propagation of membrane lateral stress, in real space and time, migrating through the different coordination shells. An extended spatiotemporal picture of collective headgroup dipole motions (b,d). The circled intensity peaks highlight areas of localized mechanical stress within otherwise relaxed neighborhoods in space and time. “Wiggling” low intensity areas (dark blue regions) feature the co-existence of different collective vibrational patterns at the water-bilayer interface.

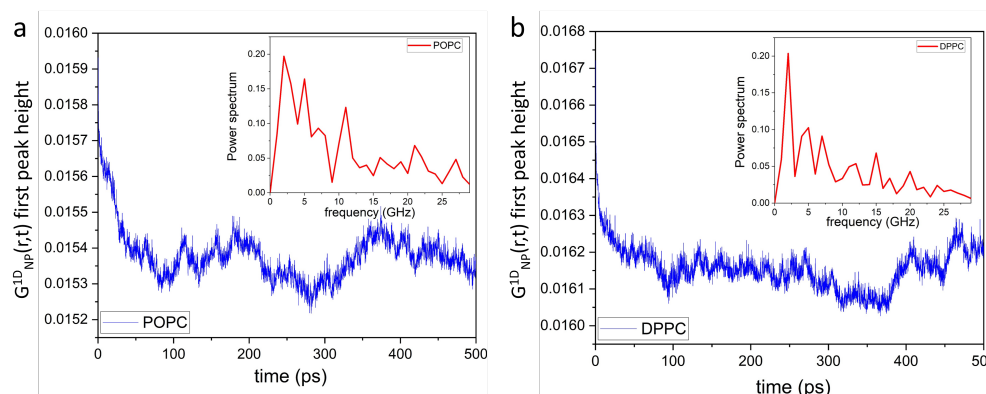


Figure 4. Time evolution of the $G_{NP}^{1D}(r, t)$ first peak height along $r \approx 0.8$ nm of lateral POPC (a) and DPPC (b) headgroup dipole spatiotemporal correlations. Insets show their respective power spectra, where their frequency bands range between ~ 2 GHz and ~ 25 GHz. Importantly, phospholipid bilayers can be externally stimulated within these frequency bands through dynamic impedance spectroscopy [57], increasing conversion efficiency of mechanical energy into electric energy.

Figure 5 shows 1D Van Hove correlation functions (see Equation (3)) of POPC (a,b) and DPPC (c,d) headgroup dipoles, characterizing their collective motions along the z-axis, i.e., $G_{NP}^{1D}(r, t)$ (Figure 1). In contrast to their lateral spatiotemporal correlations (Figure 3), the red intensity band is continuously filled (0–0.15 nm), the result of continuous stretching and squeezing elastic deformations of the headgroup dipoles (Figure 5). Moreover, out-of-plane dipole motions evolve continuously in time (see red intensity band), where the

highest intensity peak fluctuates at around 0.1 nm (see red line). The white intensity line located at ~ 0.16 nm defines the transient edge phase of headgroup dipole correlations, with a smooth oscillatory behavior taking place between ~ 0.12 nm and ~ 0.18 nm—no correlations are observed beyond 0.2 nm. Interestingly, both intensity lines (red and white) evolve coherently in time, implying that headgroup dipoles experience collective tilting, which generate surface waves or lipid bilayer surface undulations [58–60].

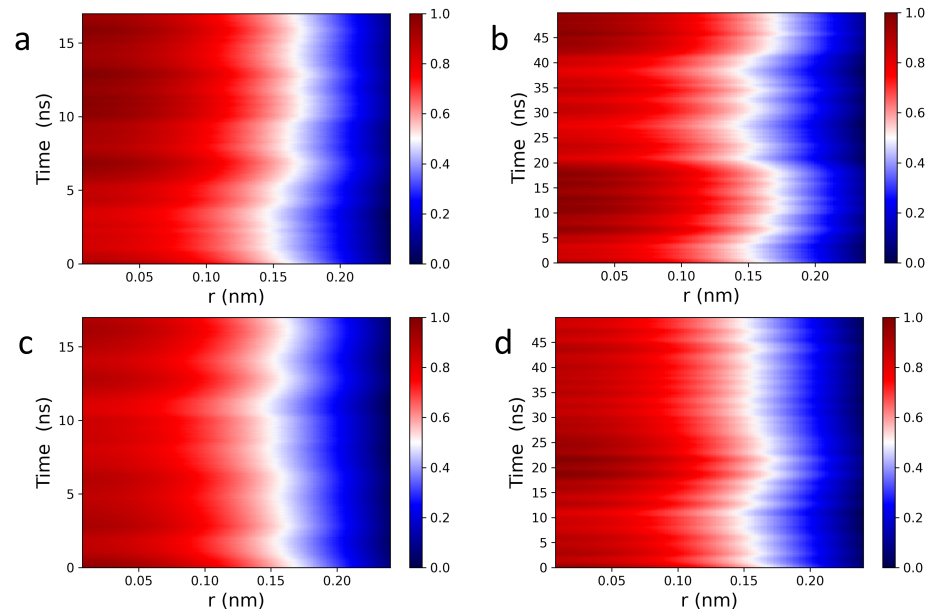


Figure 5. Spatiotemporal images of POPC (a,b) and DPPC (c,d) headgroup dipoles (along the z axis, see Figure 1) correlations calculated from Equation (1). Headgroup dipoles experience squeezing and stretching motions, filling the red intensity band from 0 nm up to 0.15 nm. The continuous, in time, oscillatory edge phase behavior of $G_{NP}^{1D}(r, t)$, implies the existence of lipid bilayer surface undulations generated by the collective tilting of headgroup dipoles.

Figure 6 shows the time evolution of the $G_{NP}^{1D}(r, t)$ first peak height of POPC (a) and DPPC (b) lipid headgroup dipoles. The insets to the figure generated using Fourier transforms, show the power spectra of the POPC and DPPC headgroup dipoles ranging between ~ 0.05 GHz and ~ 0.5 GHz. Such continuous collective movements of lipids in a bilayer are known as membrane surface undulations and play important roles in different biological processes [61–63].

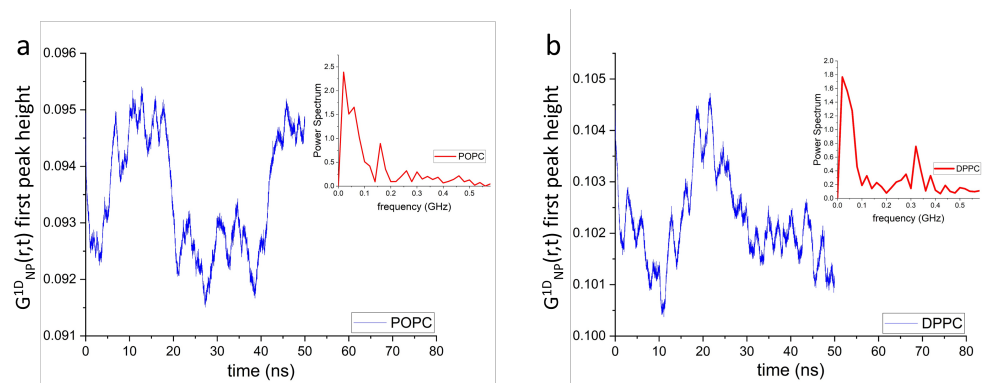


Figure 6. Time evolution of the $G_{NP}^{1D}(r, t)$ first peak height of POPC (a) and DPPC (b) headgroup dipole correlations along the z-axis. Insets show the power spectra of the $G_{NP}^{1D}(r, t)$ first peak height, where their frequency bands range between ~ 0.05 GHz and ~ 0.5 GHz. It is worth noting that lipid bilayers can be stimulated at these frequencies using dynamic impedance spectroscopy [57]. Doing so, may help to increase the conversion efficiency of mechanical energy into electric energy.

3.2. Dipole-Dipole Interactions in Lipid Bilayers

We estimated the individual vibrational frequency of neighboring lipids due to their dipole-dipole interactions along the z -axis. Specifically, we considered two lipid molecules from the inner and outer bilayer leaflets oscillating along the z -axis. The oscillating frequency of the pair of PC headgroup dipoles can be estimated from the following expression:

$$m \frac{d^2z}{dt^2} = -\frac{dV}{dz}, \quad (4)$$

where $m = 760$ and 734 are the masses of the POPC and DPPC molecules, respectively, and V is the dipole-dipole interaction potential. The first order derivative (right term in Equation (4)) is taken at the average distance between the dipoles. The potential produces a restoring force F that tends to relax at the dipoles' rest positions. The force F can then be estimated as

$$F = -\frac{dV}{dz} \sim -\frac{p^2}{4\pi\epsilon_0\epsilon z^4}, \quad (5)$$

where $p = ql$ is the dipole moment of a headgroup, q is the elementary charge, $l \approx 0.55$ nm is the average distance between the choline and phosphate ($N - P$) beads (Figure 1), and ϵ (ϵ_0) is the dielectric constant (vacuum permittivity). The angular frequency ω of dipole-dipole oscillations can be written as:

$$\omega = \sqrt{\frac{p^2}{4\pi\epsilon_0\epsilon mr^5}}, \quad (6)$$

where $r \approx 4.5$ nm is the average distance between the dipoles. Therefore, $\omega \approx 2 \times 10^{-9} \text{ s}^{-1}$ and subsequently its vibrational frequency $f = \frac{2\pi}{\omega} = 0.32$ GHz. Finally, this estimated value (0.32 GHz) of the dipole-dipole vibrational frequency is within the frequency range of both POPC and DPPC headgroup dipoles (see insets to Figure 6) calculated using MD simulations, implying that such dipole-dipole interactions contribute to the generation of lipid bilayer surface undulations.

4. Discussion and Conclusions

Biological membranes have recently been shown that they may be good systems for understanding the processing efficiency of the human brain [64]. In this regard, lipid membranes can also be utilized as neuromorphic platforms (e.g., artificial neural networks and memory computing crossbar architectures) [65–67]. For example, in neuroscience, long-term potentiation (LTP) is a long-lasting form of synaptic plasticity leading to formation, compartmentalization, and consolidation of biological memory [68]. A recent study showed that PC bilayers enable the formation of LTP mimicking the hippocampal LTP [69], previously observed in mammals and birds [70]. These memory effects can be stimulated in phospholipid membranes in response to external stimuli in the form of cyclic electric fields [57]. In this regard, piezoelectricity—a conversion of mechanical energy of lipids into electric energy, may play a major role underpinning the molecular mechanisms of memcapacitive energy storage that results in the formation of LTP [69]. Indeed, phospholipid bilayers are capable of supporting such flexoelectric and piezoelectric effects, which are stimulated by mechanical (compression and shearing), electric, optical, and magnetic stimuli, inducing the squeezing, stretching, and tilting of lipid molecules [71–75]. In this regard, the knowledge about intrinsically collective lipid motions may help us to better understand the flexoelectric and piezoelectric properties of lipid bilayers in the presence of external stimuli [76–84].

In this manuscript, we have provided spatiotemporal imaging of zwitterionic lipid bilayer collective motions, which can potentially be stimulated by external stimuli, by matching the bilayer's vibrational frequencies, thus enhancing its piezoelectric effects [57]. Specifically, we introduced 1D, 2D, and 3D Van Hove correlation functions to visualize intrinsic headgroup dipole motions. 2D and 3D spatiotemporal imaging was shown to be consistent

with common vibrational features observed in liquid systems. 1D analysis was then applied to study lateral and out-of-plane dipole motions, revealing their unique vibrational patterns. Lateral collective motions of headgroup dipoles experience ultrafast—2–4 ps—rattling dynamics, followed by long-lasting relaxation events (up to 25 ps). The extended space and time imaging of such motions showed that mechanical stress is capable of propagating back and forth, bouncing between neighboring lipid dipoles as a function of time. Mechanical stress exists in the form of localized compression and shear waves. The subsequent relaxation events enabled the release of mechanical stress, propagating it forward (both spatially and temporally), and dissipating it in the form of heat at longer times. Remarkably, the same headgroup dipoles also generated collective lipid bilayer surface undulations at ns time scales, as revealed by our 1D out-of-plane analysis. In contrast to lateral ps transient caging dynamics, out-of-plane collective dipole tilting generated continuous long-lasting—ns time scale—membrane surface undulations.

Author Contributions: Conceptualization, D.B., C.P.C. and T.E.; methodology, D.B., D.Z. and T.E.; software, D.B. and D.Z.; formal analysis, D.B., D.Z. and T.E.; writing—original draft preparation, D.B.; writing—review and editing, D.B., C.P.C., D.Z., T.E. and J.K.; funding acquisition, D.B. All authors have read and agreed to the published version of the manuscript.

Funding: This research was funded by the National Science Foundation, Division of Molecular and Cellular Biosciences (MCB), under contract no. 2219289.

Institutional Review Board Statement: Not applicable.

Acknowledgments: We are indebted to Maxim Lavrentovich for critical reading of the manuscript. D.B. is supported through the National Science Foundation, Division of Molecular and Cellular Biosciences (MCB), under contract no. 2219289. T.E. is supported by the U. S. Department of Energy, Office of Science, Basic Energy Sciences, Materials Sciences and Engineering Division. J.K. and C.P.C. are supported through the Scientific User Facilities Division of the DOE Office of Basic Energy Sciences (BES), under contract no. DE-AC05 00OR2275. Portions of the computational aspects of this research were supported by the Center for Nanophase Materials Sciences (CNMS), which is a US Department of Energy, Office of Science User Facility at Oak Ridge National Laboratory.

Conflicts of Interest: The authors declare no conflict of interest.

References

1. Luyet, C.; Elvati, P.; Vinh, J.; Violi, A. Low-THz Vibrations of Biological Membranes. *Membranes* **2023**, *13*, 139. [[CrossRef](#)] [[PubMed](#)]
2. Gupta, S.; Ashkar, R. The dynamic face of lipid membranes. *Soft Matter* **2021**, *17*, 6910–6928. [[CrossRef](#)] [[PubMed](#)]
3. Ahmadi, D.; Thompson, K.C.; García Sakai, V.; Schweins, R.; Moulin, M.; Haertlein, M.; Strohmeier, G.A.; Pichler, H.; Forsyth, V.T.; Barlow, D.J.; et al. Nanoscale structure and dynamics of model membrane lipid raft systems, studied by neutron scattering methods. *Front. Phys.* **2022**, *11*, 326. [[CrossRef](#)]
4. D'Angelo, G.; Nibali, V.C.; Wanderlingh, U.; Branca, C.; De Francesco, A.; Sacchetti, F.; Petrillo, C.; Paciaroni, A. Multiple interacting collective modes and phonon gap in phospholipid membranes. *J. Phys. Chem. Lett.* **2018**, *9*, 4367–4372. [[CrossRef](#)] [[PubMed](#)]
5. Sharma, V.; Mamontov, E. Multiscale lipid membrane dynamics as revealed by neutron spectroscopy. *Prog. Lipid Res.* **2022**, *87*, 101179. [[CrossRef](#)] [[PubMed](#)]
6. Surovtsev, N.; Adichtchev, S. Dynamic response on a nanometer scale of binary phospholipid-cholesterol vesicles: Low-frequency Raman scattering insight. *Phys. Rev. E* **2021**, *104*, 054406. [[CrossRef](#)] [[PubMed](#)]
7. Soloviov, D.; Cai, Y.Q.; Bolmatov, D.; Suvorov, A.; Zhernenkov, K.; Zav'yalov, D.; Bosak, A.; Uchiyama, H.; Zhernenkov, M. Functional lipid pairs as building blocks of phase-separated membranes. *Proc. Natl. Acad. Sci. USA* **2020**, *117*, 4749–4757. [[CrossRef](#)]
8. Anishkin, A.; Loukin, S.H.; Teng, J.; Kung, C. Feeling the hidden mechanical forces in lipid bilayer is an original sense. *Proc. Natl. Acad. Sci. USA* **2014**, *111*, 7898–7905. [[CrossRef](#)]
9. Aponte-Santamaría, C.; Brunken, J.; Gräter, F. Stress propagation through biological lipid bilayers in silico. *J. Am. Chem. Soc.* **2017**, *139*, 13588–13591. [[CrossRef](#)]
10. Bolmatov, D.; Kinnun, J.J.; Katsaras, J.; Lavrentovich, M.O. Phonon-mediated lipid raft formation in biological membranes. *Chem. Phys. Lipids* **2020**, *232*, 104979. [[CrossRef](#)]

11. Mondal, D.; Malik, S.; Banerjee, P.; Kundu, N.; Debnath, A.; Sarkar, N. Modulation of membrane fluidity to control interfacial water structure and dynamics in saturated and unsaturated phospholipid vesicles. *Langmuir* **2020**, *36*, 12423–12434. [[CrossRef](#)] [[PubMed](#)]
12. Bullerjahn, J.T.; von Bülow, S.; Hummer, G. Optimal estimates of self-diffusion coefficients from molecular dynamics simulations. *J. Chem. Phys.* **2020**, *153*, 024116. [[CrossRef](#)] [[PubMed](#)]
13. Vorobyov, I.; Olson, T.E.; Kim, J.H.; Koeppe, R.E.; Andersen, O.S.; Allen, T.W. Ion-induced defect permeation of lipid membranes. *Biophys. J.* **2014**, *106*, 586–597. [[CrossRef](#)] [[PubMed](#)]
14. Eremchev, M.; Roesel, D.; Poojari, C.S.; Roux, A.; Hub, J.S.; Roke, S. Passive transport of Ca²⁺ ions through lipid bilayers imaged by wide-field second harmonic microscopy. *Biophys. J.* **2023**, *122*, 624–631. [[CrossRef](#)]
15. Bolmatov, D.; Carrillo, J.M.Y.; Sumpter, B.G.; Katsaras, J.; Lavrentovich, M.O. Double membrane formation in heterogeneous vesicles. *Soft Matter* **2020**, *16*, 8806–8817. [[CrossRef](#)]
16. Baczynski, K.; Markiewicz, M.; Pasenkiewicz-Gierula, M. Is the tilt of the lipid head group correlated with the number of intermolecular interactions at the bilayer interface? *FEBS Lett.* **2018**, *592*, 1507–1515. [[CrossRef](#)]
17. Ray, A.; Gräter, F.; Thukral, L. Probing molecular forces in multi-component physiological membranes. *Phys. Chem. Chem. Phys.* **2018**, *20*, 2155–2161. [[CrossRef](#)]
18. Friedman, R.; Khalid, S.; Aponte-Santamaría, C.; Arutyunova, E.; Becker, M.; Boyd, K.J.; Christensen, M.; Coimbra, J.T.; Concilio, S.; Daday, C.; et al. Understanding conformational dynamics of complex lipid mixtures relevant to biology. *J. Membr. Biol.* **2018**, *251*, 609–631. [[CrossRef](#)]
19. Wang, Y.; Guo, Y.; Li, G.; Liu, C.; Wang, L.; Zhang, A.; Yan, Z.; Song, C. The push-to-open mechanism of the tethered mechanosensitive ion channel NompC. *eLife* **2021**, *10*, e58388. [[CrossRef](#)]
20. Daday, C.; de Groot, B.L. Lipid–protein forces predict conformational changes in a mechanosensitive channel. *Eur. Biophys. J.* **2021**, *50*, 181–186. [[CrossRef](#)]
21. Bolmatov, D. The Phonon Theory of Liquids and Biological Fluids: Developments and Applications. *J. Phys. Chem. Lett.* **2022**, *13*, 7121–7129. [[CrossRef](#)] [[PubMed](#)]
22. Bolmatov, D.; Zav'yalov, D.; Zhernenkov, M.; Musae, E.T.; Cai, Y.Q. Unified phonon-based approach to the thermodynamics of solid, liquid and gas states. *Ann. Phys.* **2015**, *363*, 221–242. [[CrossRef](#)]
23. Bolmatov, D.; Musae, E.T.; Trachenko, K. Symmetry breaking gives rise to energy spectra of three states of matter. *Sci. Rep.* **2013**, *3*, 2794. [[CrossRef](#)] [[PubMed](#)]
24. Bolmatov, D.; Brazhkin, V.; Trachenko, K. The phonon theory of liquid thermodynamics. *Sci. Rep.* **2012**, *2*, 421. [[CrossRef](#)]
25. Javanainen, M.; Melcrová, A.; Magarkar, A.; Jurkiewicz, P.; Hof, M.; Jungwirth, P.; Martinez-Seara, H. Two cations, two mechanisms: Interactions of sodium and calcium with zwitterionic lipid membranes. *Chem. Commun.* **2017**, *53*, 5380–5383. [[CrossRef](#)] [[PubMed](#)]
26. Melcr, J.; Martinez-Seara, H.; Nencini, R.; Kolafa, J.; Jungwirth, P.; Ollila, O.S. Accurate binding of sodium and calcium to a POPC bilayer by effective inclusion of electronic polarization. *J. Phys. Chem. B* **2018**, *122*, 4546–4557. [[CrossRef](#)]
27. McClintic, W.T.; Scott, H.L.; Moore, N.; Farahat, M.; Maxwell, M.; Schuman, C.D.; Bolmatov, D.; Barrera, F.N.; Katsaras, J.; Collier, C.P. Heterosynaptic plasticity in biomembrane memristors controlled by pH. *MRS Bulletin* **2022**, *48*, 13–21. [[CrossRef](#)]
28. Deplazes, E.; Tafalla, B.D.; Murphy, C.; White, J.; Cranfield, C.G.; Garcia, A. Calcium ion binding at the lipid–water interface alters the ion permeability of phospholipid bilayers. *Langmuir* **2021**, *37*, 14026–14033. [[CrossRef](#)]
29. Shamaeva, D.V.; Okotrub, K.A.; Surovtsev, N.V. Coexistence of lipid phases in multilayer phospholipid films probed by Raman mapping. *Analyst* **2022**, *147*, 3748–3755. [[CrossRef](#)]
30. Walde, P.; Ichikawa, S. Lipid vesicles and other polymolecular aggregates—from basic studies of polar lipids to innovative applications. *Appl. Sci.* **2021**, *11*, 10345. [[CrossRef](#)]
31. Bolmatov, D.; McClintic, W.T.; Taylor, G.; Stanley, C.B.; Do, C.; Collier, C.P.; Leonenko, Z.; Lavrentovich, M.O.; Katsaras, J. Deciphering melatonin-stabilized phase separation in phospholipid bilayers. *Langmuir* **2019**, *35*, 12236–12245. [[CrossRef](#)] [[PubMed](#)]
32. Yang, J.; Jin, J.; Li, S. Role of polyunsaturated phospholipids in liquid-ordered and liquid-disordered phases. *RSC Adv.* **2021**, *11*, 27115–27120. [[CrossRef](#)] [[PubMed](#)]
33. Liu, R.; Chen, Y.; Yang, L.; Bie, M.; Wang, B. Role of lipid rafts in persistent *Helicobacter pylori* infection: A narrative review. *Ann. Transl. Med.* **2022**, *10*, 376. [[CrossRef](#)] [[PubMed](#)]
34. Bolmatov, D.; Lavrentovich, M.; Reiter, R.J. Molecular interactions of melatonin with lipid rafts. *Mel. Res.* **2022**, *5*, 101–113. [[CrossRef](#)]
35. Karathanou, K.; Bondar, A.N. Dynamic water hydrogen-bond networks at the interface of a lipid membrane containing palmitoyl-oleoyl phosphatidylglycerol. *J. Membr. Biol.* **2018**, *251*, 461–473. [[CrossRef](#)]
36. Srivastava, A.; Debnath, A. Hydration dynamics of a lipid membrane: Hydrogen bond networks and lipid-lipid associations. *J. Chem. Phys.* **2018**, *148*, 094901. [[CrossRef](#)]
37. Conti Nibali, V.; Branca, C.; Wanderlingh, U.; D'Angelo, G. Intermolecular Hydrogen-Bond Interactions in DPPE and DMPC Phospholipid Membranes Revealed by Far-Infrared Spectroscopy. *Appl. Sci.* **2021**, *11*, 10038. [[CrossRef](#)]
38. Katsaras, J. X-ray diffraction studies of oriented lipid bilayers. *Biochem. Cell Biol.* **1995**, *73*, 209–218. [[CrossRef](#)]

39. Kučerka, N.; Nagle, J.F.; Sachs, J.N.; Feller, S.E.; Pencer, J.; Jackson, A.; Katsaras, J. Lipid bilayer structure determined by the simultaneous analysis of neutron and X-ray scattering data. *Biophys. J.* **2008**, *95*, 2356–2367. [[CrossRef](#)]
40. Marquardt, D.; Frontzek, M.D.; Zhao, Y.; Chakoumakos, B.C.; Katsaras, J. Neutron diffraction from aligned stacks of lipid bilayers using the WAND instrument. *J. Appl. Crystallogr.* **2018**, *51*, 235–241. [[CrossRef](#)]
41. Marrink, S.J.; Tieleman, D.P. Perspective on the Martini model. *Chem. Soc. Rev.* **2013**, *42*, 6801–6822. [[CrossRef](#)] [[PubMed](#)]
42. Jo, S.; Kim, T.; Iyer, V.G.; Im, W. CHARMM-GUI: A web-based graphical user interface for CHARMM. *J. Comput. Chem.* **2008**, *29*, 1859–1865. [[CrossRef](#)] [[PubMed](#)]
43. Wu, E.L.; Cheng, X.; Jo, S.; Rui, H.; Song, K.C.; Dávila-Contreras, E.M.; Qi, Y.; Lee, J.; Monje-Galvan, V.; Venable, R.M.; et al. CHARMM-GUI membrane builder toward realistic biological membrane simulations. *J. Comput. Chem.* **2014**, *35*, 1997–2004. [[CrossRef](#)] [[PubMed](#)]
44. Van Hove, L. Correlations in space and time and Born approximation scattering in systems of interacting particles. *Phys. Rev.* **1954**, *95*, 249. [[CrossRef](#)]
45. Egami, T.; Shinohara, Y. Correlated atomic dynamics in liquid seen in real space and time. *J. Chem. Phys.* **2020**, *153*, 180902. [[CrossRef](#)] [[PubMed](#)]
46. Iwashita, T.; Wu, B.; Chen, W.R.; Tsutsui, S.; Baron, A.Q.; Egami, T. Seeing real-space dynamics of liquid water through inelastic x-ray scattering. *Sci. Adv.* **2017**, *3*, e1603079. [[CrossRef](#)]
47. Shinohara, Y.; Osaka, T.; Inoue, I.; Iwashita, T.; Dmowski, W.; Ryu, C.W.; Sarathchandran, Y.; Egami, T. Split-pulse X-ray photon correlation spectroscopy with seeded X-rays from X-ray laser to study atomic-level dynamics. *Nat. Commun.* **2020**, *11*, 6213. [[CrossRef](#)]
48. Dmowski, W.; Diallo, S.O.; Lokshin, K.; Ehlers, G.; Ferré, G.; Boronat, J.; Egami, T. Observation of dynamic atom-atom correlation in liquid helium in real space. *Nat. Commun.* **2017**, *8*, 15294. [[CrossRef](#)]
49. Shinohara, Y.; Ivanov, A.S.; Maltsev, D.; Granroth, G.E.; Abernathy, D.L.; Dai, S.; Egami, T. Real-Space Local Dynamics of Molten Inorganic Salts Using Van Hove Correlation Function. *J. Phys. Chem. Lett.* **2022**, *13*, 5956–5962. [[CrossRef](#)]
50. Katsaras, J.; Tristram-Nagle, S.; Liu, Y.; Headrick, R.; Fontes, E.; Mason, P.; Nagle, J.F. Clarification of the ripple phase of lecithin bilayers using fully hydrated, aligned samples. *Phys. Rev. E* **2000**, *61*, 5668. [[CrossRef](#)]
51. Ashcraft, R.; Wang, Z.; Abernathy, D.; Quirinale, D.; Egami, T.; Kelton, K. Experimental determination of the temperature-dependent Van Hove function in a Zr80Pt20 liquid. *J. Chem. Phys.* **2020**, *152*, 074506. [[CrossRef](#)] [[PubMed](#)]
52. Zhernenkov, M.; Bolmatov, D.; Soloviov, D.; Zhernenkov, K.; Toperverg, B.P.; Cunsolo, A.; Bosak, A.; Cai, Y.Q. Revealing the mechanism of passive transport in lipid bilayers via phonon-mediated nanometre-scale density fluctuations. *Nat. Commun.* **2016**, *7*, 11575. [[CrossRef](#)] [[PubMed](#)]
53. Bolmatov, D.; Cai, Y.Q.; Zav'yalov, D.; Zhernenkov, M. Crossover from picosecond collective to single particle dynamics defines the mechanism of lateral lipid diffusion. *Biochim. Biophys. Acta (BBA)-Biomembr.* **2018**, *1860*, 2446–2455. [[CrossRef](#)] [[PubMed](#)]
54. Bolmatov, D.; Soloviov, D.; Zhernenkov, M.; Zav'yalov, D.; Mamontov, E.; Suvorov, A.; Cai, Y.Q.; Katsaras, J. Molecular picture of the transient nature of lipid rafts. *Langmuir* **2020**, *36*, 4887–4896. [[CrossRef](#)]
55. Bolmatov, D.; Zhernenkov, M.; Zav'yalov, D.; Stoupin, S.; Cai, Y.Q.; Cunsolo, A. Revealing the mechanism of the viscous-to-elastic crossover in liquids. *J. Phys. Chem. Lett.* **2015**, *6*, 3048–3053. [[CrossRef](#)] [[PubMed](#)]
56. Bolmatov, D.; Zhernenkov, M.; Zav'yalov, D.; Stoupin, S.; Cunsolo, A.; Cai, Y.Q. Thermally triggered phononic gaps in liquids at THz scale. *Sci. Rep.* **2016**, *6*, 19469. [[CrossRef](#)] [[PubMed](#)]
57. Sacci, R.L.; Scott, H.L.; Liu, Z.; Bolmatov, D.; Doughty, B.; Katsaras, J.; Collier, C.P. Disentangling memristive and memcapacitive effects in droplet interface bilayers using dynamic impedance spectroscopy. *Adv. Electron. Mater.* **2022**, *8*, 2200121. [[CrossRef](#)]
58. Lindahl, E.; Edholm, O. Mesoscopic undulations and thickness fluctuations in lipid bilayers from molecular dynamics simulations. *Biophys. J.* **2000**, *79*, 426–433. [[CrossRef](#)]
59. Haataja, M.P. Lipid domain co-localization induced by membrane undulations. *Biophys. J.* **2017**, *112*, 655–662. [[CrossRef](#)]
60. Monzel, C.; Sengupta, K. Measuring shape fluctuations in biological membranes. *J. Phys. D Appl. Phys.* **2016**, *49*, 243002. [[CrossRef](#)]
61. Bradley, R.P.; Radhakrishnan, R. Curvature–undulation coupling as a basis for curvature sensing and generation in bilayer membranes. *Proc. Natl. Acad. Sci. USA* **2016**, *113*, E5117–E5124. [[CrossRef](#)] [[PubMed](#)]
62. Molaei, M.; Kandy, S.K.; Graber, Z.T.; Baumgart, T.; Radhakrishnan, R.; Crocker, J.C. Probing lipid membrane bending mechanics using gold nanorod tracking. *Phys. Rev. Res.* **2022**, *4*, L012027. [[CrossRef](#)] [[PubMed](#)]
63. Pinigin, K.V. Determination of Elastic Parameters of Lipid Membranes with Molecular Dynamics: A Review of Approaches and Theoretical Aspects. *Membranes* **2022**, *12*, 1149. [[CrossRef](#)] [[PubMed](#)]
64. Najem, J.S.; Hasan, M.S.; Williams, R.S.; Weiss, R.J.; Rose, G.S.; Taylor, G.J.; Sarles, S.A.; Collier, C.P. Dynamical nonlinear memory capacitance in biomimetic membranes. *Nat. Commun.* **2019**, *10*, 3239. [[CrossRef](#)]
65. Ball, P. Soft learning. *Nat. Mater.* **2023**, *22*, 2. [[CrossRef](#)]
66. Xiong, T.; Li, C.; He, X.; Xie, B.; Zong, J.; Jiang, Y.; Ma, W.; Wu, F.; Fei, J.; Yu, P.; et al. Neuromorphic functions with a polyelectrolyte-confined fluidic memristor. *Science* **2023**, *379*, 156–161. [[CrossRef](#)]
67. Robin, P.; Emmerich, T.; Ismail, A.; Niguès, A.; You, Y.; Nam, G.H.; Keerthi, A.; Siria, A.; Geim, A.; Radha, B.; et al. Long-term memory and synapse-like dynamics in two-dimensional nanofluidic channels. *Science* **2023**, *379*, 161–167. [[CrossRef](#)]
68. Nicoll, R.A. A brief history of long-term potentiation. *Neuron* **2017**, *93*, 281–290. [[CrossRef](#)]

69. Scott, H.L.; Bolmatov, D.; Podar, P.T.; Liu, Z.; Kinnun, J.J.; Doughty, B.; Lydic, R.; Sacci, R.L.; Collier, C.P.; Katsaras, J. Evidence for long-term potentiation in phospholipid membranes. *Proc. Natl. Acad. Sci. USA* **2022**, *119*, e2212195119. [[CrossRef](#)]
70. Bliss, T.V.; Lømo, T. Long-lasting potentiation of synaptic transmission in the dentate area of the anaesthetized rabbit following stimulation of the perforant path. *Physiol. J.* **1973**, *232*, 331–356. [[CrossRef](#)]
71. Harden, J.; Diorio, N.; Petrov, A.G.; Jakli, A. Chirality of lipids makes fluid lamellar phases piezoelectric. *Phys. Rev. E* **2009**, *79*, 011701. [[CrossRef](#)] [[PubMed](#)]
72. Jákli, A.; Harden, J.; Notz, C.; Bailey, C. Piezoelectricity of phospholipids: A possible mechanism for mechanoreception and magnetoreception in biology. *Liq. Cryst.* **2008**, *35*, 395–400. [[CrossRef](#)]
73. Huang, H.; Delikanli, S.; Zeng, H.; Ferkey, D.M.; Pralle, A. Remote control of ion channels and neurons through magnetic-field heating of nanoparticles. *Nat. Nanotechnol.* **2010**, *5*, 602–606. [[CrossRef](#)]
74. Mosgaard, L.D.; Zecchi, K.A.; Heimburg, T. Mechano-capacitive properties of polarized membranes. *Soft Matter* **2015**, *11*, 7899–7910. [[CrossRef](#)] [[PubMed](#)]
75. Chen, R.; Romero, G.; Christiansen, M.G.; Mohr, A.; Anikeeva, P. Wireless magnetothermal deep brain stimulation. *Science* **2015**, *347*, 1477–1480. [[CrossRef](#)] [[PubMed](#)]
76. Shapiro, M.G.; Homma, K.; Villarreal, S.; Richter, C.P.; Bezanilla, F. Infrared light excites cells by changing their electrical capacitance. *Nat. Commun.* **2012**, *3*, 736. [[CrossRef](#)] [[PubMed](#)]
77. Freeman, E.; Najem, J.; Sukharev, S.; Philen, M.; Leo, D. The mechano-electrical response of droplet interface bilayer membranes. *Soft Matter* **2016**, *12*, 3021–3031. [[CrossRef](#)]
78. Bolmatov, D.; Zhernenkov, M.; Sharpnack, L.; Agra-Kooijman, D.M.; Kumar, S.; Suvorov, A.; Pindak, R.; Cai, Y.Q.; Cunsolo, A. Emergent optical phononic modes upon nanoscale mesogenic phase transitions. *Nano Lett.* **2017**, *17*, 3870–3876. [[CrossRef](#)]
79. Plaksin, M.; Shapira, E.; Kimmel, E.; Shoham, S. Thermal transients excite neurons through universal intramembrane mechano-electrical effects. *Phys. Rev. X* **2018**, *8*, 011043. [[CrossRef](#)]
80. Bolmatov, D.; Soloviov, D.; Zav'yalov, D.; Sharpnack, L.; Agra-Kooijman, D.M.; Kumar, S.; Zhang, J.; Liu, M.; Katsaras, J. Anomalous nanoscale optoacoustic phonon mixing in nematic mesogens. *J. Phys. Chem. Lett.* **2018**, *9*, 2546–2553. [[CrossRef](#)]
81. Thomas, N.; Agrawal, A. Quantification of in-plane flexoelectricity in lipid bilayers. *Europhys. Lett.* **2021**, *134*, 68003. [[CrossRef](#)]
82. Kim, T.; Kadji, H.; Whalen, A.J.; Ashourvan, A.; Freeman, E.; Fried, S.I.; Tadigadapa, S.; Schiff, S.J. Thermal effects on neurons during stimulation of the brain. *J. Neural Eng.* **2022**, *19*, 056029. [[CrossRef](#)] [[PubMed](#)]
83. Thomas, N.; Agrawal, A. A lateral electric field inhibits gel-to-fluid transition in lipid bilayers. *Soft Matter* **2022**, *18*, 6437–6442. [[CrossRef](#)] [[PubMed](#)]
84. Heimburg, T. The excitable fluid mosaic. *Biochim. Biophys. Acta (BBA)-Biomembr.* **2023**, *1865*, 184104. [[CrossRef](#)] [[PubMed](#)]

Disclaimer/Publisher's Note: The statements, opinions and data contained in all publications are solely those of the individual author(s) and contributor(s) and not of MDPI and/or the editor(s). MDPI and/or the editor(s) disclaim responsibility for any injury to people or property resulting from any ideas, methods, instructions or products referred to in the content.